Truncated optical Bessel modes

K. Koksal [1,*] M. Babiker [2] V. E. Lembessis [3] and J. Yuan [2]

[1]*Physics Department, Bitlis Eren University, Bitlis 13000, Turkey*

[2]*Department of Physics, University of York, York YO10 5DD, United Kingdom*

[3]*Quantum Technology Group, Department of Physics and Astronomy, College of Science, King Saud University, Riyadh 11451, Saudi Arabia*

(Received 8 March 2022; accepted 24 May 2022; published 16 June 2022)

An orthonormal set of optical vortex modes is put forward and identified as the polarized truncated optical Bessel (TOB) set, which is endowed with orbital as well as spin angular momentum. Members of this set of modes can be realized once a circular aperture of radius R is placed centrally in the path of an optical Bessel beam of winding number ℓ. For a fixed power input $\mathcal{P}$, the properties of the TOB set, namely, its helicity, energy, linear momentum, and spin and orbital angular momenta, are evaluated, and their main features are explored. The similarities and differences between the properties of the TOB mode set and those of the Laguerre-Gaussian set are pointed out and discussed.

DOI: 10.1103/PhysRevA.105.063512

I. INTRODUCTION

Free-space optical Bessel modes form one class of vortex modes characterized by orbital angular momentum as well as spin. Their electric field is an exact solution of the Helmholtz equation $\nabla^2\mathbf{E} + (\omega^2/c^2)\mathbf{E} = 0$. In cylindrical polar coordinates $\mathbf{r} = (\rho, \phi, z)$ the electric field of the Bessel mode has the form

$$\mathbf{E}(\mathbf{r}, t) = \mathcal{E}_0\hat{\mathbf{e}}J_\ell(\kappa\rho)e^{i\ell\phi}e^{ik_z z}e^{-i\omega t}. \tag{1}$$

Here the unit vector $\hat{\mathbf{e}}$ represents wave polarization, $\mathcal{E}_0$ is a normalization factor, and J_ℓ is the Bessel function of the first kind of order ℓ and frequency ω; the wave numbers k_z and κ are the axial (longitudinal) and radial (transverse) components of the total wave vector $\mathbf{k}$ such that $k = \sqrt{(k_z^2 + \kappa^2)}$. As a form of structured light [1], the optical Bessel modes have received considerable attention both theoretically and experimentally, with a number of prominent applications, including the controlled manipulation of small particles [2–5].

It is, however, well understood that such an unbounded "free-space" optical Bessel mode J_ℓ of frequency ω propagating along the $+z$ axis with an axial wave number k_z is not realizable in practice since it would need an infinite amount of energy. One method to realize it, albeit approximately, is to use an aperture of radius R which is large relative to the wavelength and so acts to isolate a sizable central part of the beam cross section.

In this paper we are concerned with a scenario in which the aperture radius R is so chosen that the Bessel argument $\kappa\rho$ at $\rho = R$ as in Eq. (1) coincides with one of the zeros λ of the Bessel function. The concept of an aperture introduced in this manner first featured in the case of Bessel electron vortex waves in an electron microscope [6]. Our optical Bessel mode is subject to a circular aperture of radius R and acquires a well-defined transverse wave number $\kappa = \lambda/R$, so that $J_{|\ell|}(\kappa R) = J_{|\ell|}(\lambda) = 0$. A zero denoted as $\lambda_{p\ell}$ is the $(p+1)$th zero of the Bessel function of order ℓ, where $p = 0, 1, 2, \ldots$ is a radial index and $\kappa^{p\ell} = \lambda_{p\ell}/R$ is the transverse (in-plane) wave number. Thus, the truncated optical Bessel (TOB) modes are characterized by two discrete indices ℓ and p, resembling in this way the two indices of Laguerre-Gaussian modes.

The optical field produced in the manner described above is derivable from a vector potential $\mathbf{A}_{p\ell}(\mathbf{r}, t)$, which, in cylindrical polar coordinates, has the form

$$\mathbf{A}_{p\ell}(\mathbf{r}, t) = (\alpha\hat{\boldsymbol{x}} + \beta\hat{\boldsymbol{y}})\mathcal{F}_{p\ell}(\rho, \phi)e^{(ik_z z - i\omega t)}, \tag{2}$$

where α and β are, in general, complex constants. The amplitude function $\mathcal{F}_{p\ell}(\rho, \phi)$ conforming with the requirements whereby the Bessel argument $\kappa^{p\ell}\rho$ at $\rho = R$ coincides with one of the zeros $\lambda_{p\ell}$ of the Bessel function is given by

$$\mathcal{F}_{p\ell}(\rho, \phi) = \mathcal{E}_0 J_{|\ell|}(\kappa^{p\ell}\rho)e^{i\ell\phi} \quad (\rho \leqslant R), \tag{3}$$

$$\mathcal{F}_{p\ell}(\rho, \phi) = 0 \qquad (\rho > R), \tag{4}$$

where $\mathcal{E}_0$ is an overall normalization factor which is fixed by the requirement that its value is consistent with an input power of known magnitude $\mathcal{P}$. The members of this set of optical vortex modes can be called truncated optical Bessel modes.

The magnetic field of the representative TOB mode emerges from $\boldsymbol{\nabla} \times \mathbf{A}$ in the exact form

$$\mathbf{B} = ik_z(\alpha\hat{\boldsymbol{y}} - \beta\hat{\boldsymbol{x}})\mathcal{F}e^{ik_z z} + \hat{\boldsymbol{z}}\left(\beta\frac{\partial\mathcal{F}}{\partial x} - \alpha\frac{\partial\mathcal{F}}{\partial y}\right)e^{ik_z z}, \tag{5}$$

where we have dropped the mode label $p\ell$ from $\mathcal{F}$ and κ and do not show the time exponential $\exp(-i\omega t)$ for ease of notation; these can be restored where required. It is easy to check that this magnetic field satisfies $\boldsymbol{\nabla} \cdot \mathbf{B} = 0$. The associated electric field must follow from the main requirement of duality such that $\mathbf{E}$ is related to $\mathbf{B}$ via the Maxwell equation for a monochromatic field, namely, $\mathbf{E} = (ic^2/\omega)\boldsymbol{\nabla} \times \mathbf{B}$.

*Corresponding author: kkoksal@beu.edu.tr

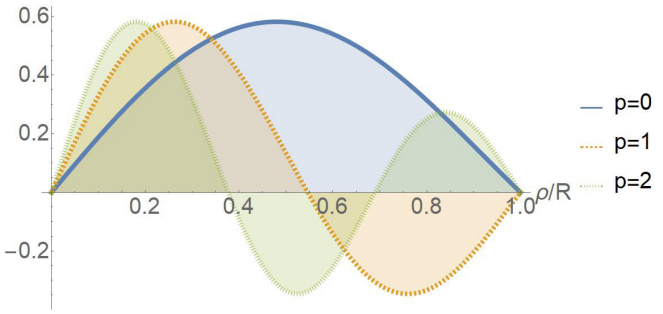

FIG. 1. The radial variations of the amplitude function for three members of the TOB set for which $\ell = 1$ and $p = 0, 1, 2$. Note that all TOB mode functions vanish at $\rho = R$, coinciding with $\lambda^{p\ell}$, the $(p+1)$th zero of the Bessel function.

Consistency demands that the electric field must be of the form

$$\mathbf{E} = ick_z(\alpha\hat{\mathbf{x}} + \beta\hat{\mathbf{y}})\mathcal{F}e^{ik_z z} - c\left\{\alpha\frac{\partial\mathcal{F}}{\partial x} + \beta\frac{\partial\mathcal{F}}{\partial y}\right\}e^{ik_z z}\hat{\mathbf{z}}. \quad (6)$$

This field satisfies $\nabla\cdot\mathbf{E} = 0$. Also, it can be verified, for consistency, that the exact field $\mathbf{B}$, Eq. (5), emerging as $\nabla\times\mathbf{A}$ must also emerge from $\mathbf{E}$ in Eq. (6) by application of the second Maxwell equation for a monochromatic field, namely, $\mathbf{B} = (1/i\omega)\nabla\times\mathbf{E}$. Note that both $\mathbf{E}$ and $\mathbf{B}$ have z (longitudinal) components in addition to the transverse x and y components.

It is straightforward to ensure that the set of TOB modes defined by Eqs. (3) and (4), denoted as

$$\{\mathcal{F}_{p\ell}(\rho,\phi)\}, \quad |\ell| = 0, 1, 2, \ldots, p = 0, 1, 2, \ldots,$$

forms a complete orthonormal set of functions in the aperture plane. The relevant integrals needed for orthonormalization are

$$\tfrac{1}{2\pi}\int_0^{2\pi} e^{i\ell\phi}e^{-i\ell'\phi}d\phi = \delta_{\ell\ell'}, \quad (7)$$

$$\int_0^R J_{|\ell|}(\kappa^{p\ell}\rho)J_{|\ell'|}(\kappa^{p'\ell'}\rho)\rho d\rho = \tfrac{R^2}{2}[J_{|\ell|+1}(\lambda_{p\ell})]^2\delta_{\ell\ell'}\delta_{pp'}. \quad (8)$$

The normalization factor $\mathcal{E}_0$ is fixed in terms of the applied power $\mathcal{P}$. Appendix A shows the details and supplies the result as follows:

$$\mathcal{E}_0^2 = \frac{2\mu_0\mathcal{P}}{c\pi k_z^2 R^2[J_{|\ell|+1}(\lambda_{p\ell})]^2}. \quad (9)$$

It is also clear that these TOB modes are eigenfunctions of the z component of the orbital-angular-momentum operator $\hat{L}_z = -i\hbar\partial/\partial\phi$ with eigenvalues $\hbar\ell$ and, like free-space Bessel modes, they are orbital-angular-momentum modes. For illustration, Fig. 1 displays the radial variations of the three TOB modes for which $\ell = +1$ but $p = 0, 1, 2$.

As is the case for all electromagnetic fields satisfying duality within Maxwell's equations, the TOB modes are characterized by the main properties, namely, optical helicity, energy, linear momentum, and spin and angular momentum. Besides identifying the set of the TOB modes, as detailed above, the goal of this paper is to explore these properties specifically for the TOB modes. We first consider the cycle-averaged densities in turn and evaluate them specifically for a general TOB mode, displaying the spatial distributions in the aperture plane and identifying contributions from the transverse- and longitudinal-field components. The next task for each property is to integrate the respective densities over the aperture plane, thereby deriving the total respective mode

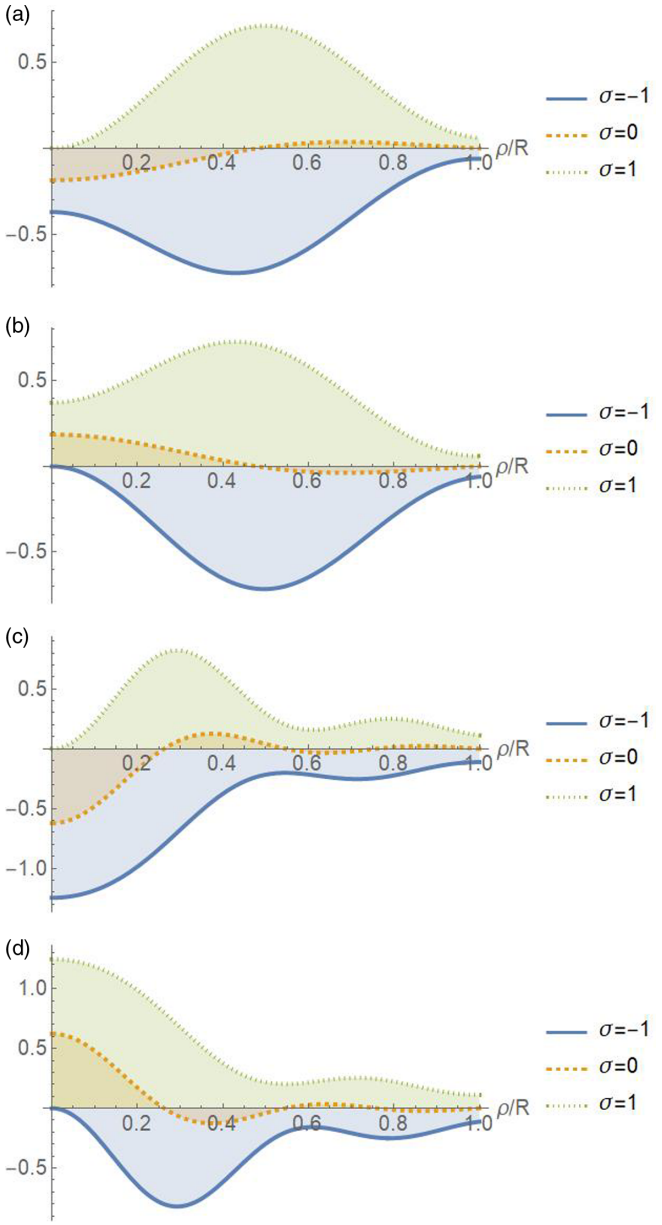

FIG. 2. The radial variations of the helicity density (in Jsm^{-3}) displayed by the TOB modes $p\ell$ with $\ell = \pm 1$ for the three cases in which $\sigma = 0, \pm 1$. (a) and (b) refer to the cases for which $p = 0$, but with $\ell = 1$ and $\ell = -1$, respectively. (c) and (d) refer to the cases for which $p = 1$, but with $\ell = 1$ and $\ell = -1$, respectively. Note that for the cases where $\sigma = \pm 1$, the helicity density does not vanish at $\rho = R$. This can be traced to the contribution of the middle term in Eq. (26), which depends on the first derivative of the Bessel function, which does not vanish at $\rho = R$. Note also how the choices of the signs of σ and ℓ lead to different shapes of the helicity-density distributions.

properties. In the Sec. VIII we summarize the main results of the work and point out their main features relative to other vortex modes.

II. CYCLE-AVERAGED DENSITIES

With the electric and magnetic fields of the truncated Bessel mode as detailed in Eqs. (2) to (6), we can now proceed (i) to evaluate the cycle-averaged helicity density $\bar{\eta}$, the Poynting vector $\bar{\boldsymbol{w}}$, the linear momentum density $\bar{\boldsymbol{\pi}}$, the optical spin angular momentum (SAM) density $\bar{\mathbf{s}}$, and the angular momentum (AM) density $\bar{\boldsymbol{j}}$ of a polarized truncated optical Bessel mode; (ii) to evaluate the cycle average per unit length of the total helicity, total energy, total SAM, and total angular momentum as space integrals over the x-y plane of the respective densities; and (iii) finally, to discuss the results obtained, with special emphasis on the roles of the wave polarization and vortex contributions to the properties.

The cycle-averaged densities are defined as follows:

$$\bar{\eta}(\mathbf{r}) = -\tfrac{\epsilon_0 c}{2\omega}\mathrm{Im}[\mathbf{E}^*\cdot\mathbf{B}] \quad \text{(helicity density)}, \tag{10}$$

$$\bar{\mathbf{w}} = \tfrac{1}{2\mu_0}\mathrm{Re}[\mathbf{E}^*\times\mathbf{B}] \quad \text{(Poynting vector)}, \tag{11}$$

$$\bar{\boldsymbol{\pi}} = \tfrac{1}{c^2}\bar{\mathbf{w}} \quad \text{(linear momentum density)}, \tag{12}$$

$$\bar{\boldsymbol{s}} = \tfrac{\epsilon_0}{\omega}\mathrm{Im}[\mathbf{E}^*\times\mathbf{E}] \quad \text{(SAM density)}, \tag{13}$$

$$\bar{\boldsymbol{j}} = \mathbf{r}\times\bar{\boldsymbol{\pi}} \quad \text{(AM density)}, \tag{14}$$

where Re[·] and Im[·] stand for the real and imaginary parts and the asterisk (*) in $\mathbf{E}^*$ stands for the complex conjugate of $\mathbf{E}$. As stated above, we deal in turn with the evaluations of the above densities specifically in relation to the TOB modes.

III. HELICITY OF TOB MODES

The cycle-averaged helicity density $\bar{\eta}$ of the TOB mode is as defined in Eq. (10). The helicity as one of the main properties of an optical mode has attracted much interest recently [7–12], and more recent accounts have revived interest in this beam property and its relation to optical spin [13–19].

Substituting the electric and magnetic fields in Eqs. (5) and (6), we have for the dot product $\mathbf{E}^*\cdot\mathbf{B}$

$$\mathbf{E}^*\cdot\mathbf{B} = ck^2(\alpha\beta^* - \beta\alpha^*)|\mathcal{F}|^2 - c\left\{\alpha^*\left(\frac{\partial\mathcal{F}}{\partial x}\right)^* + \beta^*\left(\frac{\partial\mathcal{F}}{\partial y}\right)^*\right\}\left(\beta\frac{\partial\mathcal{F}}{\partial x} - \alpha\frac{\partial\mathcal{F}}{\partial y}\right), \tag{15}$$

where, for ease of notation, we do not show the labels $p\ell$ and the argument ρ, ϕ in the field function $\mathcal{F}$, as defined in Eq. (3). In Eq. (15) we identify the derivative terms as contributions to the helicity density due to the z components (longitudinal components). Multiplying out in the second term, we obtain

$$\mathbf{E}^*\cdot\mathbf{B} = ck^2(\alpha\beta^* - \beta\alpha^*)|\mathcal{F}|^2 - c\left\{\beta\alpha^*\left|\frac{\partial\mathcal{F}}{\partial x}\right|^2 - \alpha\beta^*\left|\frac{\partial\mathcal{F}}{\partial y}\right|^2 + |\beta|^2\left(\frac{\partial\mathcal{F}}{\partial x}\right)\left(\frac{\partial\mathcal{F}}{\partial y}\right)^* - |\alpha|^2\left(\frac{\partial\mathcal{F}}{\partial x}\right)^*\left(\frac{\partial\mathcal{F}}{\partial y}\right)\right\}. \tag{16}$$

As $\mathcal{F}$ is a function of (ρ, ϕ), it is straightforward to evaluate the x and y derivatives. We obtain, not showing the labels $(p\ell)$ in κ,

$$\left(\frac{\partial\mathcal{F}}{\partial x}\right) = (\mathcal{Q}\cos\phi - i\mathcal{T}\sin\phi) \tag{17}$$

and

$$\left(\frac{\partial\mathcal{F}}{\partial y}\right) = (\mathcal{Q}\sin\phi + i\mathcal{T}\cos\phi), \tag{18}$$

where $\mathcal{Q}$ and $\mathcal{T}$ are given by

$$\mathcal{Q} = \mathcal{E}_0\kappa J'_{|\ell|}e^{i\ell\phi}, \quad \mathcal{T} = \mathcal{E}_0\frac{\ell}{\rho}J_{|\ell|}e^{i\ell\phi}, \tag{19}$$

where $J'_{|\ell|}(s)$ is the first derivative $d[J_{|\ell|}(s)]/ds$. Without loss of generality we now restrict considerations to the cases in which the complex parameters α and β conform with the following identities:

$$|\alpha|^2 + |\beta|^2 = 1, \quad \alpha\beta^* - \beta\alpha^* = 2i\mathrm{Im}[\alpha\beta^*]. \tag{20}$$

So we then have

$$\sigma = i(\alpha\beta^* - \alpha^*\beta) = 2\alpha\beta', \tag{21}$$

where we have set $\beta = i\beta'$. We shall consider two cases. (a) The linear polarization case is as follows:

$$\alpha = 1, \quad \beta = 0, \quad \text{so } \sigma = 0. \tag{22}$$

(b) The circular polarization case is such that

$$\alpha = 1/\sqrt{2}, \quad \beta = i/\sqrt{2}, \quad \text{so } \sigma \neq 0. \tag{23}$$

We now explore the helicity properties of cases (a) and (b). Continuing with the evaluation of the general helicity density, we obtain for the dot product $\mathbf{E}^*\cdot\mathbf{B}$ after some algebra

$$\mathbf{E}^*\cdot\mathbf{B} = -i\sigma ck_z^2|J_{|\ell|}|^2 - c\left\{\frac{1}{2}i\sigma(\mathcal{Q}^2 + \mathcal{T}^2) - i\mathcal{Q}\mathcal{T}\right\}. \tag{24}$$

Thus, we find for the cycle-averaged helicity density

$$\bar{\eta} = \mathcal{E}_0^2\frac{\epsilon_0 c^2}{4\omega}\left\{\sigma\left(2k_z^2|J_{|\ell|}|^2 + \mathcal{Q}^2 + \mathcal{T}^2\right) - 2\mathcal{Q}\mathcal{T}\right\}. \tag{25}$$

The first term is the σ-dependent helicity density of the transverse-field components, and we can now see that the longitudinal fields are responsible for adding the terms $(\mathcal{Q}^2 + \mathcal{T}^2)$ to the σ-dependent part of the helicity density and they give rise to a σ-independent, but ℓ-dependent, contribution to the density in the term $-2\mathcal{Q}\mathcal{T}$. It is convenient at this stage to

substitute for $\mathcal{T}$ and obtain

$$\bar{\eta} = \mathcal{E}_0^2 \frac{\epsilon_0 c^2}{4\omega} \left\{ \sigma \left[2k_z^2 |J_{|\ell|}|^2 + (\kappa J'_{|\ell|})^2 + \left(\frac{\ell}{\rho} |J_{|\ell|}| \right)^2 \right] - \ell \left(\frac{2\kappa J'_{|\ell|} J_{|\ell|}}{\rho} \right) \right\}, \tag{26}$$

where the arguments in all functions are $(\kappa^{p\ell}\rho)$. This is the general form of the helicity density of the circularly polarized TOB mode, as defined above. Recall that the mode is characterized by the winding number ℓ and radial number p. The helicity density consists of two distinct contributions: the first, denoted $\bar{\eta}_\sigma$, is associated with wave polarization and is proportional to σ. The second, denoted $\bar{\eta}_{\ell,p,0}$, is given by the second term. This is a σ-independent contribution associated with the orbital-angular-momentum vortex. Characteristically, it is proportional to the vortex winding number ℓ. Thus, we can write the helicity density of the most general TOB beam as the sum of the two contributions as follows:

$$\bar{\eta} = \bar{\eta}_\sigma + \bar{\eta}_{\ell,p,0}, \tag{27}$$

where $\bar{\eta}_\sigma$ is the expression in Eq. (26) that is proportional to σ. We have

$$\bar{\eta}_\sigma = \mathcal{E}_0^2 \frac{\epsilon_0 c^2}{4\omega} \sigma \left[2k_z^2 |J_{|\ell|}|^2 + \kappa^2 |J'_{|\ell|}|^2 + \left(\frac{|\ell|}{\rho} |J_{|\ell|}| \right)^2 \right]. \tag{28}$$

The rest of the expression in Eq. (26) defines $\bar{\eta}_{\ell,p,0}$,

$$\begin{aligned} \bar{\eta}_{\ell,p,0} &= -\ell \mathcal{E}_0^2 \frac{\epsilon_0 c^2}{4\omega} \left(\frac{2\kappa J'_{|\ell|} J_{|\ell|}}{\rho} \right) \\ &= -\ell \mathcal{E}_0^2 \frac{\epsilon_0 c^2}{4\omega\rho} \kappa J_{|\ell|} \{ J_{|\ell|-1} - J_{|\ell|+1} \}. \end{aligned} \tag{29}$$

The helicity-density term $\bar{\eta}_{\ell,p,0}$ is nonzero when $\sigma = 0$, i.e., for a linearly polarized TOB mode. This σ-independent helicity density stems only from the longitudinal-field components and is directly proportional to the winding number ℓ and changes sign when the winding number changes sign. For example, the helicity-density distributions $\bar{\eta}_{1,0,0}(\rho)$ and $\bar{\eta}_{-1,0,0}(\rho)$ of two linearly polarized TOB modes which differ only in their winding numbers ℓ are such that $\bar{\eta}_{1,0,0}(\rho) = -\bar{\eta}_{-1,0,0}(\rho)$ for all radial positions ρ in the aperture plane. This is shown clearly by the orange dashed curves in Figs. 2(a) and 2(b), and the same applies for the cases for the orange dashed curves in Figs. 2(c) and 2(d) for which $p = 1$. As the cycle-averaged helicity density is directly proportional to the chirality density, this change in sign confirms that linearly polarized TOB modes are characterized by a handedness, i.e., exhibit a chiral behavior [20].

IV. INTEGRATED HELICITY

A. Linear polarization

Note that the helicity-density distribution is, in general, nonzero at points in the aperture plane. Using standard integrals, we obtain the total helicity per unit length for a linearly polarized TOB mode ($\sigma = 0$). Thus, we have

$$\begin{aligned} \bar{\mathcal{C}}_{\ell,p,0} &= \int_0^{2\pi} d\phi \int_0^R \rho \, d\rho \, \bar{\eta}_{\ell,p,0} \\ &= -\ell \mathcal{E}_0^2 \tfrac{\epsilon_0 c^2}{4\omega} \int_0^{2\pi} d\phi \int_0^R \left(\tfrac{2\kappa^{p\ell} J_{|\ell|}(\kappa^{p\ell}\rho) J'_{|\ell|}(\kappa^{p\ell}\rho)}{\rho} \right) \rho \, d\rho. \end{aligned} \tag{30}$$

The integral can be dealt with as follows. Let $x = \kappa^{p\ell}\rho$, and we have $\kappa^{p\ell} R = \lambda_{p\ell}$; then

$$\begin{aligned} \kappa^{p\ell} \int_0^R J_{|\ell|}(\kappa^{p\ell}\rho) J'_{|\ell|}(\kappa^{p\ell}\rho) d\rho &= \int_0^{\lambda_{p\ell}} J_{|\ell|}(x) J'_{|\ell|}(x) dx \\ &= \tfrac{1}{2} \int_0^{\lambda_{p\ell}} \tfrac{d}{dx} [J_{|\ell|}(x)]^2 dx = [J_{|\ell|}(\lambda_{p\ell})]^2/2 = 0. \end{aligned} \tag{31}$$

Thus, we have reached the conclusion that, although the helicity density of a linearly polarized TOB mode has a nonzero distribution which exhibits chirality, its space integral $\bar{\mathcal{C}}_{\ell,p,0}$ vanishes identically for all TOB modes. The statement that $\bar{\mathcal{C}}_{\ell,p,0} = 0$ is the first of our main results in this paper. It asserts that without optical spin an optical vortex alone cannot produce total helicity, even though it exhibits helicity-density distributions, which in turn indicates that on radial integration the different parts of the density distribution are canceled out by other parts. A similar observation in the case of Laguerre-Gaussian modes was pointed out recently [19].

B. CIRCULAR POLARIZATION

The total helicity for a circularly polarized TOB is obtained by integrating over the density in Eq. (26). We have, restoring the notation in the Bessel functions,

$$\mathcal{C}_{\ell p,\sigma} = \mathcal{E}_0^2 \frac{\epsilon_0 c^2}{4\omega} \int_0^{2\pi} d\phi \int_0^R \left\{ \sigma \left[2k_z^2 |J_{|\ell|}(\kappa^{p\ell}\rho)|^2 + [\kappa^{p\ell} J'_{|\ell|}(\kappa^{p\ell}\rho)]^2 + \left(\frac{\ell}{\rho} |J_{|\ell|}(\kappa^{p\ell}\rho)| \right)^2 \right] - \ell \left(\frac{2\kappa^{p\ell} J_{|\ell|}(\kappa^{p\ell}\rho) J'_{|\ell|}(\kappa^{p\ell}\rho)}{\rho} \right) \right\} \rho \, d\rho. \tag{32}$$

As shown in Eq. (31) integrating the last term in Eq. (32) gives zero. Dropping the last term, we have for the total helicity

$$\mathcal{C}_{\ell p,\sigma} = \sigma \mathcal{E}_0^2 \frac{\epsilon_0 c^2}{4\omega} \int_0^{2\pi} d\phi \int_0^R \left\{ 2k_z^2 |J_{|\ell|}(\kappa^{p\ell}\rho)|^2 + [\kappa^{p\ell} J'_{|\ell|}(\kappa^{p\ell}\rho)]^2 + \left(\frac{\ell}{\rho} |J_{|\ell|}(\kappa^{p\ell}\rho)| \right)^2 \right\} \rho \, d\rho. \tag{33}$$

The evaluation of Eq. (33) is detailed in Appendix C. The result is as follows:

$$\mathcal{C}_{\ell p,\sigma} = \sigma \mathcal{E}_0^2 \frac{\pi \epsilon_0 c^2}{2\omega} \{ I_1 + (I_2 + I_3) \}, \tag{34}$$

where I_1, I_2, and I_3 are, respectively, the first, second, and third integrals in Eq. (33). Appendix C supplies the results for these integrals. We find on substitution from Eq. (C8)

$$\mathcal{C}_{\ell p,\sigma} = \sigma \mathcal{E}_0^2 \frac{\pi \epsilon_0 c^2 k_z^2 R^2}{2\omega} \left\{ 1 + \frac{\lambda_{p\ell}^2}{2k_z^2 R^2} \right\} [J_{|\ell|+1}(\lambda_{p\ell})]^2. \tag{35}$$

Substituting $\mathcal{E}_0$ from Eq. (A5), we can write the total helicity per unit length as

$$\mathcal{C}_{\ell,p,\sigma} = \sigma L_0 \left\{ 1 + \frac{\lambda_{p\ell}^2}{2k_z^2 R^2} \right\}, \tag{36}$$

where L_0 has the dimensions of angular momentum per unit length,

$$L_0 = \frac{\mathcal{P}}{\omega c}. \tag{37}$$

We identify Eq. (36) as the second of our main results. It is easy to check that for a large $R \to \infty$ the second term in Eq. (36) is zero and total helicity becomes $\mathcal{C}_{\ell,p,\sigma} = \sigma L_0$, which coincides with the helicity of a free Bessel mode. We show below that the total axial spin angular momentum of the TOB mode is $\bar{S}_z = \sigma L_0$. This suggests that the helicity for the TOB mode as given by Eq. (36) differs from that of the free-space Bessel mode by the additional second term, so it no longer coincides with the optical spin.

V. ENERGY MOMENTUM OF THE TOB MODE

The components of the cycle-averaged Poynting vector $\bar{\mathbf{w}}$ are formally given by

$$\bar{\mathbf{w}}_i = \frac{1}{2\mu_0} \epsilon_{ijk} \mathrm{Re}[E_j^* B_k]. \tag{38}$$

Substituting the fields in Eqs. (5) and (6) and making use of the Cartesian derivatives in Eqs. (17), (18), and (19), we find after some algebra

$$\bar{\mathbf{w}}_x = -\frac{c}{2\mu_0} \left\{ \frac{k_z \ell}{\rho} \sin\phi |J_{|\ell|}|^2 - 2ik_z \alpha\beta^* J_{|\ell|} \mathcal{Q} \sin\phi \right\}, \tag{39}$$

$$\bar{\mathbf{w}}_y = \frac{c}{2\mu_0} \left\{ \frac{k_z \ell}{\rho} \cos\phi |J_{|\ell|}|^2 + 2ik_z \alpha^* \beta J_{|\ell|} \mathcal{Q} \cos\phi \right\}, \tag{40}$$

$$\bar{\mathbf{w}}_z = \frac{c}{2\mu_0} k_z^2 |J_{|\ell|}|^2 \mathcal{E}_0^2, \tag{41}$$

where we have assumed circular polarization and so have made use of the relations in Eqs. (20) and (21).

The linear-momentum-density vector $\bar{\boldsymbol{\pi}}$ is given by Eq. (12), with components proportional to the Poynting-vector components, so they can readily be deduced from the components in Eqs. (39) to (41). These $\bar{\boldsymbol{\pi}}$ components enable the evaluation of the total angular momentum, as we show in the next section.

The cycle-averaged energy density is obtained on multiplying the z component of the linear momentum density by the velocity of light, so the TOB mode energy per unit length is the integral over the aperture plane. We have

$$\bar{U} = \int_0^{2\pi} d\phi \int_0^R \left[c \frac{\bar{\mathbf{w}}_z}{c^2} \right] \rho \, d\rho. \tag{42}$$

Substituting $\bar{\mathbf{w}}_z$ in Eq. (41), we find

$$\bar{U} = \frac{\pi k_z^2 \mathcal{E}_0^2}{c\mu_0} \int_0^R |J_{|\ell|}(\kappa^{p\ell}\rho)|^2 \rho \, d\rho, \tag{43}$$

which yields

$$\bar{U} = \mathcal{E}_0^2 \frac{\pi c k_z^2 R^2}{2c\mu_0} [J_{|\ell|+1}(\lambda_{p\ell})]^2 \tag{44}$$

Substituting $\mathcal{E}_0$ from Eq. (A5), we find in terms of the input power $\mathcal{P}$

$$\bar{U} = \frac{\mathcal{P}}{c}, \tag{45}$$

which has the dimensions of energy per unit length.

VI. ANGULAR MOMENTUM OF THE TOB MODE

The cycle-averaged angular-momentum-density vector of the TOB mode is given by Eq. (14), which is

$$\bar{j} = \mathbf{r} \times \bar{\mathbf{w}}/c^2 = \frac{1}{2\mu_0 c^2} \mathbf{r} \times \mathrm{Re}[\mathbf{E}^* \times \mathbf{B}] \tag{46}$$

The three components of the angular-momentum-density vector can be evaluated on the focal plane by substituting directly from Eqs. (39) to (41). We obtain for the x component

$$\bar{j}_x = \rho \sin\phi \bar{\mathbf{w}}_z = \frac{c k_z^2 \mathcal{E}_0^2}{2\mu_0} |J_{|\ell|}|^2 \rho \sin\phi. \tag{47}$$

Similarly, we have for the y component

$$\bar{j}_y = -\rho \cos\phi \bar{\mathbf{w}}_z = -\frac{c k_z^2 \mathcal{E}_0^2}{2\mu_0} |J_{|\ell|}|^2 \rho \cos\phi, \tag{48}$$

and we note that these transverse components are ϕ dependent. Finally, we evaluate the z component and obtain, using Eqs. (39) and (40),

$$\bar{j}_z = \mathcal{E}_0^2 \frac{c k_z}{2\mu_0 c^2} \{ \ell |J_{|\ell|}|^2 - \rho\sigma\kappa J_{|\ell|} J'_{|\ell|} \}. \tag{49}$$

The total AM per unit length of the three angular momentum components is defined as the two-dimensional space integral of the respective densities. It is easy to see that on integrating $\bar{j}_x$ and $\bar{j}_y$ we obtain zero in each case by virtue of a vanishing ϕ integral. We therefore write

$$\bar{\mathcal{J}}_x = 0 = \bar{\mathcal{J}}_y. \tag{50}$$

Thus, we conclude that although the transverse angular momentum displays density distributions, their total space integrals vanish identically. However, the z component is nonvanishing on integration. We have, restoring the notation on the Bessel functions,

$$\bar{\mathcal{J}}_z = \mathcal{E}_0^2 \frac{c k_z \pi}{\mu_0 c^2} \int_0^R \{ \ell |J_{|\ell|}(\kappa^{p\ell}\rho)|^2 - \rho\sigma\kappa^{p\ell} J_{|\ell|}(\kappa^{p\ell}\rho) J'_{|\ell|}(\kappa^{p\ell}\rho) \} \rho \, d\rho. \tag{51}$$

The evaluations of the integrals are shown in Appendix B. We have, with $\kappa^{p\ell} = \lambda^{p\ell}/R$,

$$\begin{aligned} \bar{\mathcal{J}}_z &= \mathcal{E}_0^2 \frac{c k_z \pi}{\mu_0 c^2} \left\{ \ell \mathcal{I}_1 - \sigma \frac{\lambda_{p\ell}}{R} \mathcal{I}_2 \right\} \\ &= \frac{R^2}{2} \mathcal{E}_0^2 \frac{c k_z \pi}{\mu_0 c^2} [J_{\ell+1}(\lambda_{p\ell})]^2 \{ \ell + \sigma \} \\ &= \mathcal{E}_0^2 \frac{\pi c k_z R^2}{2\mu_0 c^2} [J_{\ell+1}(\lambda_{p\ell})]^2 \{ \ell + \sigma \}. \end{aligned} \tag{52}$$

Substituting for $\mathcal{E}_0$ from Eq. (A5) we have

$$\bar{\mathcal{J}}_z = \frac{\pi c k_z R^2}{2\mu_0 c^2} [J_{\ell+1}(\lambda_{p\ell})]^2 \{ \ell + \sigma \} \frac{2\mu_0 \mathcal{P}}{c\pi k_z^2 R^2 [J_{\ell+1}(\lambda_{p\ell})]^2}. \tag{53}$$

We obtain, finally, on performing the cancellations

$$\bar{\mathcal{J}}_z = \frac{\mathcal{P}}{c^2 k_z}\{\ell+\sigma\} = \tilde{L}\{\ell+\sigma\}, \tag{54}$$

where $\tilde{L}$ has the dimensions of angular momentum per unit length. We have, using $\omega = ck$ and $k_z = \sqrt{k^2 - (\kappa^{p\ell})^2}$,

$$\tilde{L} = L_0/\sqrt{1-(\kappa^{p\ell})^2 c^2/\omega^2}, \tag{55}$$

where

$$L_0 = \frac{\mathcal{P}}{\omega c}. \tag{56}$$

The ratio of angular momentum per unit length and energy per unit length follows immediately from Eqs. (54) and (45),

$$\frac{\bar{\mathcal{J}}_z}{\bar{U}} = \frac{\{\ell+\sigma\}\mathcal{P}/(k_z c^2)}{\mathcal{P}/c} = \frac{\ell+\sigma}{\omega\sqrt{1-(\kappa^{p\ell})^2 c^2/\omega^2}}. \tag{57}$$

This result differs from the corresponding result given by Allen *et al.* [21] by the square-root-factor term in the denominator which depends on $\kappa^{p\ell} = \lambda_{p\ell}/R$. Thus, for large R we recover the standard result $(\ell+\sigma)/\omega$. The total-angular-momentum axial component per unit length of the TOB mode is the sum $(\ell+\sigma)$ multiplied by the angular momentum factor $\tilde{L}$, which differs from L_0 by the same square-root factor. The constant L_0 enters the helicity and, also enters the axial spin angular momentum of the TOB mode. It follows that the spin and orbital angular momenta are coupled for the TOB mode, and furthermore, as we have shown above, the helicity does not coincide with the axial spin angular momentum. The square-root factor in the denominator of Eq. (54) suggests that the axial angular momentum increases with diminishing R. This result may well be amenable to experimental verification.

VII. SPIN ANGULAR MOMENTUM

The cycle-averaged optical spin-angular-momentum density is as defined in Eq. (13),

$$\bar{\boldsymbol{s}}_{\ell,p,\sigma} = \frac{\epsilon_0}{2\omega}\mathrm{Im}[\mathbf{E}^* \times \mathbf{E}], \tag{58}$$

where the TOB mode electric field is as given by Eq. (6). All three components of $\bar{\boldsymbol{s}}_{\ell,p,\sigma}$ can be evaluated. Consider the x component

$$\begin{aligned}[\mathbf{E}^* \times \mathbf{E}]_x &= (E_y^* E_z - E_z^* E_y)\\ &= ic^2 k_z\left\{\beta^*\alpha\mathcal{F}^*\left(\frac{\partial\mathcal{F}}{\partial x}\right) + \alpha^*\beta\mathcal{F}\left(\frac{\partial\mathcal{F}}{\partial x}\right)^*\right\} + ic^2 k_z|\beta|^2\left\{\mathcal{F}^*\left(\frac{\partial\mathcal{F}}{\partial y}\right) + \mathcal{F}\left(\frac{\partial\mathcal{F}}{\partial y}\right)^*\right\}.\end{aligned} \tag{59}$$

Substituting the derivatives in Eqs. (17) and (18), we find for the x component of the SAM density

$$\begin{aligned}\bar{s}_x &= \frac{\epsilon_0}{2\omega}\mathrm{Im}[\mathbf{E}^* \times \mathbf{E}]_x\\ &= -\frac{c^2 k_z \epsilon_0}{2\omega}\mathcal{E}_0^2\left\{\sigma\frac{\ell}{\rho}|J_{|\ell|}|^2 - \kappa J'_{|\ell|}J_{|\ell|}\right\}\sin\phi.\end{aligned} \tag{60}$$

The y component of the SAM density follows in a similar fashion. We have

$$[\mathbf{E}^* \times \mathbf{E}]_y = E_z^* E_x - E_x^* E_z = -ic^2 k_z\left\{\alpha\beta^*\mathcal{F}\left(\frac{\partial\mathcal{F}}{\partial y}\right)^* + \alpha^*\beta\mathcal{F}^*\left(\frac{\partial\mathcal{F}}{\partial y}\right) + |\alpha|^2\left[\mathcal{F}\left(\frac{\partial\mathcal{F}}{\partial x}\right)^* + \mathcal{F}^*\left(\frac{\partial\mathcal{F}}{\partial x}\right)\right]\right\}. \tag{61}$$

Then the y component of the SAM density is

$$\begin{aligned}\bar{s}_y &= \frac{\epsilon_0}{2\omega}\mathrm{Im}[\mathbf{E}^* \times \mathbf{E}]_y\\ &= -\frac{c^2 k_z \epsilon_0}{2\omega}\mathcal{E}_0^2\left\{\sigma\frac{\ell}{\rho}|J_{|\ell|}|^2 - \kappa J'_{|\ell|}J_{|\ell|}\right\}\cos\phi.\end{aligned} \tag{62}$$

It is interesting to note that the transverse density components $\bar{s}_x$ and $\bar{s}_y$ both display distributions in the focal plane and each shows a spin-orbit term. However, all terms in these SAM densities turn out to be proportional to the sine or cosine of the azimuthal coordinate ϕ. As we show below, the space integrals of these transverse density components both vanish identically because of the angular integral.

Finally, we consider the SAM z component. We have

$$\begin{aligned}[\mathbf{E}^* \times \mathbf{E}]_z &= (E_x^* E_y - E_y^* E_x)\\ &= k^2(\alpha^*\beta - \alpha\beta^*) = i\sigma k^2|\mathcal{F}|^2,\end{aligned} \tag{63}$$

so that the z component of the SAM density is

$$\bar{s}_z = \frac{\epsilon_0}{2\omega}\mathrm{Im}[\mathbf{E}^* \times \mathbf{E}]_z = \frac{k^2\epsilon_0 c^2}{2\omega}\sigma|\mathcal{F}|^2. \tag{64}$$

The total (integrated) SAM density components are obtained by integration over the aperture plane. We have for the transverse components at once

$$\bar{S}_x = 0 = \bar{S}_y. \tag{65}$$

The vanishing of $\bar{S}_x$ and $\bar{S}_y$ follows the pattern of the transverse components of the angular momentum, as discussed earlier [Eq. (50)]. As in the case of angular momentum, the only surviving SAM component is the z component, which yields, on integrating the z component of the SAM density,

$$\bar{S}_z = 2\mathcal{E}_0^2\pi\frac{k_z^2\epsilon_0 c^2}{2\omega}\sigma\int_0^R |J_{|\ell|}(\kappa^{p\ell}\rho)|^2\rho d\rho. \tag{66}$$

We proceed to evaluate $\bar{S}_z$ by making use of the standard integrals

$$\int_0^R J_{|\ell|}(\kappa^{p\ell}\rho)J_{|\ell|}(\kappa^{p'\ell}\rho)\rho\, d\rho = R^2\frac{\delta_{pp'}}{2}[J_{|\ell|+1}(\lambda_{p\ell})]^2. \quad (67)$$

We then have

$$\bar{S}_z = 2\mathcal{E}_0^2\pi\frac{k_z^2\epsilon_0 c^2}{2\omega}\sigma\frac{R^2}{2}[J_{|\ell|+1}(\lambda_{p\ell})]^2, \quad (68)$$

which is

$$\bar{S}_z = \sigma\mathcal{E}_0^2\frac{\pi k_z^2 R^2\epsilon_0 c^2}{2\omega}[J_{|\ell|+1}(\lambda_{p\ell})]^2. \quad (69)$$

But from Appendix A we have for $\mathcal{E}_0$

$$\mathcal{E}_0^2 = \frac{2\mu_0\mathcal{P}}{c\pi k_z^2 R^2[J_{|\ell|+1}(\lambda_{p\ell})]^2}, \quad (70)$$

which leads, after cancellations, to the cycle-averaged axial component of SAM,

$$\bar{S}_z = \sigma\left(\frac{\mathcal{P}}{\omega c}\right) = \sigma L_0, \quad (71)$$

and we note the same overall factor L_0 in the optical spin angular momentum. As the result in Eq. (71) is independent of the aperture radius R, it applies also to the free-space Bessel modes. Furthermore, the result is the same as for the total SAM of a Laguerre-Gaussian mode.

VIII. COMMENTS AND CONCLUSIONS

We have focused on the electromagnetic modes arising from the physical constraints due to the application of an aperture on Bessel modes, and we have compared and contrasted their properties with those of Laguerre-Gaussian modes. The use of an aperture is commonplace in beam-shaping techniques. Most laser systems operate in their fundamental mode, and typically, spatial light modulators (SLMs) and other beam-shaping devices are used. In higher-power applications, beam shaping using an SLM of a finite size would lead to a low power efficiency. Truncation allows a uniform beam input in order to maximize the power throughput of the SLM without damaging it. Truncation also arises naturally as in biological experiments where small holes are used to isolate the excitation volume of a broad beam illumination in a single molecular fluorescence experiment.

Our aim here has been to study the properties of optical modes which arise when Bessel modes are subject to an aperture which is chosen so that the radius of the aperture coincides with a zero of the mode Bessel function, leading to what we termed truncated Bessel modes. We pointed out that the TOB modes form an orthonormal set of modes in the aperture plane and proceeded to evaluate in turn their optical properties.

One of our main results states that the helicity $\bar{\mathcal{C}}_{\ell,p,0}$ given by Eq. (31) is identically zero for all linearly polarized TOB modes. This asserts that with $\sigma = 0$ any linearly polarized optical TOB mode alone cannot give rise to a nonzero total helicity, even though it exhibits nonzero helicity-density distributions. This in turn indicates that on radial integration the different parts of the density distribution are canceled out by other parts. A similar observation in the case of Laguerre-Gaussian modes was pointed out recently [19].

Our second main result is stated in Eq. (36) for the total helicity when $\sigma \neq 0$. It is easy to check that for a large $R \to \infty$ the second term in Eq. (36) is zero and total helicity becomes $\bar{\mathcal{C}}_{\ell,p,\sigma} = \sigma L_0$, which coincides with the helicity of a free Bessel mode. We have also shown that the total optical axial spin angular momentum of the TOB mode is $\bar{S}_z = \sigma L_0$. This suggests that the helicity for the TOB mode as given by Eq. (36) differs from that of the free-space Bessel mode by the additional second term and it no longer coincides with the axial optical spin angular momentum.

In our third main set of results in Eqs. (54) to (57), we have shown that the ratio of total angular momentum to energy per unit length differs from the corresponding standard result given by Allen *et al.* [21] by a square-root-factor term which depends on $\kappa^{p\ell} = \lambda_{p\ell}/R$. Thus, for large R we recover the standard result $(\ell + \sigma)/\omega$. The total-angular-momentum axial component per unit length of the TOB mode is the sum $(\ell + \sigma)$ multiplied by the angular momentum factor $\tilde{L}$, which differs by the same square-root factor from L_0 which enters the helicity and, also enters the axial spin angular momentum of the TOB mode. It follows that the spin and orbital angular momenta are coupled for the TOB mode, and as we have shown above, the helicity does not coincide with the axial spin angular momentum. The square-root factor in the denominator of Eq. (54) suggests that the axial angular momentum increases with diminishing R. This result may well be amenable to experimental verification.

Although we have shown that the total (integrated) transverse components of the SAM (namely, $\bar{S}_x$ and $\bar{S}_y$) and the transverse components of the optical angular momentum $\bar{\mathcal{J}}_x$ and $\bar{\mathcal{J}}_y$ all vanish identically and so could all be understood to have no role to play in the vortex beam characteristics, there has been considerable emphasis recently on the significant roles which the nonvanishing transverse density distributions $\bar{s}_x$ and $\bar{s}_y$ and $\bar{j}_x$ and $\bar{j}_y$ of twisted light play in a number of scenarios. Such densities are considered to lead to various applications, including optical chirality in the interaction with chiral matter, optical sensing of biosystems, near-field microscopy, plasmonic devices, and the manipulation of atoms and molecules as well as the control of bulk matter at the nanoscale [22,23].

The significance of the total helicity result of the TOB mode, namely, Eq. (36), is worth a separate comment. The second term in the brackets in this equation stems directly from the presence of the longitudinal-field components. This term increases with diminishing radius R. For a TOB mode of given ℓ, p this term becomes greater than or equal to unity for R values satisfying

$$\lambda^{p\ell} \geqslant \sqrt{2}k_z R = 2\sqrt{2}\pi\frac{R}{\Lambda}, \quad (72)$$

where Λ is the wavelength. As an example we consider the case $\ell = 1$. Table I shows the zeros of the TOB modes for which $\ell = 1$. Clearly, as the TOB radial number p increases, the second term in Eq. (36) can equal or exceed unity when the Bessel zero equals or exceeds the right-hand side of Eq. (72) and the value of the helicity more than doubles in magnitude. This is a manifestation of the inclusion of the longitudinal-

TABLE I. The $(p+1)$th zeros of the $\ell = 1$ Bessel function $J_1(s)$ for $p = 0$ to 4.

$(p+1, \ell = 1)$	λ^{p1}
1	3.83
2	7.01
3	10.17
4	13.32
5	16.47
...	...

field components, and since it is ℓ dependent, the second helicity term is essentially a spin-orbit term which vanishes when $\ell = 0$.

Finally, it should be remembered that we have focused only on the beam properties in the focal plane at $z = 0$. The question arises as to what properties the beam is destined to have in other planes with $z > 0$ along the axis as influenced by diffraction. However, an investigation of the effects of the beam propagation on the beam properties, albeit interesting, is beyond the scope of this paper, but in general, we expect the densities of the helicity, spin, orbital, and linear momenta of the truncated Bessel beam to change as the diffraction alters the beam profile. In contrast, we expect the corresponding integrated (total) properties will not change. This issue is not considered any further in this paper.

ACKNOWLEDGMENTS

K.K. wishes to thank Tubitak and Bitlis Eren University for financial support (under project BEBAP 2021.10) during his sabbatical year at the University of York where this work was initiated.

The authors declare no conflicts of interest.

APPENDIX A: THE NORMALIZATION FACTOR $\mathcal{E}_0$

The overall normalization factor which appears in the form of the truncated optical Bessel mode is evaluated in terms of the average power $\mathcal{P}$, which is the surface integral of the average Poynting vector $\mathbf{E}^* \times \mathbf{B}/2\mu_0$ over the aperture plane. The surface element is $\mathbf{d\Sigma} = d\Sigma\hat{\mathbf{z}}$, so only the z component of the Poynting vector enters the integration,

$$\mathcal{P} = \frac{1}{2\mu_0}\int_0^{2\pi} d\phi \int_0^R |(\mathbf{E}^* \times \mathbf{B})_z|\rho d\rho. \tag{A1}$$

The z component of the Poynting vector is given by

$$\frac{1}{2\mu_0}\mathrm{Re}[\mathbf{E}^* \times \mathbf{B}]_z = \frac{c\mathcal{E}_0^2}{2\mu_0}k_z^2|J_{|\ell|}|^2. \tag{A2}$$

Thus, we have

$$\mathcal{P} = \mathcal{E}_0^2\left(\frac{\pi c k_z^2}{\mu_0}\right)\int_0^R |J_{|\ell|}(\kappa\rho)|^2\rho d\rho. \tag{A3}$$

We can then make use of the standard integral

$$\int_0^R J_{|\ell|}(\kappa^{p\ell}\rho)J_{|\ell|}(\kappa^{p'\ell}\rho)\rho\, d\rho = R^2\frac{\delta_{pp'}}{2}[J_{|\ell|+1}(\lambda_{p\ell})]^2 \tag{A4}$$

and so obtain, finally, for the normalization factor $\mathcal{E}_0$

$$\mathcal{E}_0^2 = \frac{2\mu_0\mathcal{P}}{c\pi k_z^2 R^2[J_{|\ell|+1}(\lambda_{p\ell})]^2}. \tag{A5}$$

It is straightforward to check that the dimensions of $\mathcal{E}_0$ are consistent with Eq. (3).

APPENDIX B: EVALUATION OF EQUATION (51)

The relevant integrals are as follows. For $\mathcal{I}_1$ we have

$$\mathcal{I}_1 = \int_0^R [J_{|\ell|}(\kappa^{p\ell}\rho)]^2\rho\, d\rho. \tag{B1}$$

Recall that $\kappa_{p\ell} = \lambda^{p\ell}/R$. Thus, we have

$$\mathcal{I}_1 = \int_0^R [J_{|\ell|}(\lambda_{p\ell}\rho/R)]^2\rho\, d\rho = \frac{R^2}{2}[J_{|\ell|+1}(\lambda_{p\ell})]^2. \tag{B2}$$

Next, we deal with $\mathcal{I}_2$, which is

$$\mathcal{I}_2 = \int_0^R J_{|\ell|}(\kappa^{p\ell}\rho)J'_{|\ell|}(\kappa^{p\ell}\rho)\rho^2\, d\rho. \tag{B3}$$

It is convenient to write $\kappa^{p\ell}\rho = x$; then $\rho = x(R/\lambda_{p\ell})$. The integral becomes

$$\begin{aligned}\mathcal{I}_2 &= \frac{R^3}{(\lambda_{p\ell})^3}\int_0^{\lambda_{p\ell}} J_{|\ell|}(x)J'_{|\ell|}(x)x^2\, dx \\ &= -\frac{R^3}{2\lambda_{p\ell}}[J_{\ell+1}(\lambda_{p\ell})]^2.\end{aligned} \tag{B4}$$

APPENDIX C: EVALUATION OF EQUATION (32)

The relevant integrals are

$$I_1 = \int_0^R \left\{2k_z^2|J_{|\ell|}(\kappa^{p\ell}\rho)|^2\right\}\rho\, d\rho, \tag{C1}$$

$$I_2 = \int_0^R [\kappa^{p\ell}J'_{|\ell|}(\kappa^{p\ell}\rho)]^2\rho\, d\rho, \tag{C2}$$

$$I_3 = \int_0^R \left(\frac{\ell}{\rho}|J_{|\ell|}(\kappa^{p\ell}\rho)|\right)^2\rho\, d\rho. \tag{C3}$$

We deal with these integrals in turn. For I_1 we make use of the standard integral in Eq. (C4). We have

$$I_1 = k_z^2R^2[J_{|\ell|+1}(\lambda_{p\ell})]^2. \tag{C4}$$

Next, consider I_2. We have

$$\begin{aligned}I_2 &= (\kappa^{p\ell})^2\int_0^R [J'_{|\ell|}(\kappa^{p\ell}\rho)]^2\rho\, d\rho \\ &= \frac{1}{4}(\kappa^{p\ell})^2\int_0^R [J_{|\ell|-1}(x) - J_{|\ell|+1}(x)]^2\rho\, d\rho.\end{aligned} \tag{C5}$$

We proceed to consider I_3. We have, using the identity $\frac{2\ell}{x} = [J_{|\ell|-1}(x) + J_{|\ell|+1}(x)]$, with $x = \kappa^{p\ell}\rho$,

$$\begin{aligned}I_3 &= \int_0^R \left(\frac{\ell}{\rho}|J_{|\ell|}(\kappa^{p\ell}\rho)|\right)^2\rho\, d\rho \\ &= \frac{1}{4}(\kappa^{p\ell})^2\int_0^R [J_{|\ell|-1}(\kappa^{p\ell}\rho) + J_{|\ell|+1}(\kappa^{p\ell}\rho)]^2\rho\, d\rho.\end{aligned} \tag{C6}$$

We can now combine the two integrals $I_2 + I_3$ to obtain

$$(I_2 + I_3) = \frac{1}{2}(\kappa^{p\ell})^2 \int_0^R \{[J_{|\ell|-1}(\kappa^{p\ell}\rho)]^2 + [J_{|\ell|+1}(\kappa^{p\ell}\rho)]^2\}\rho\, d\rho = \frac{1}{2}\lambda_{p\ell}^2 [J_{|\ell|+1}(\lambda_{p\ell})]^2. \quad \text{(C7)}$$

The sum of integrals is then given by

$$I_1 + (I_2 + I_3) = \left\{k_z^2 R^2 + \frac{1}{2}\lambda_{p\ell}^2\right\}[J_{|\ell|+1}(\lambda_{p\ell})]^2. \quad \text{(C8)}$$

[1] H. Rubinsztein-Dunlop, A. Forbes, M. V. Berry, M. R. Dennis, D. L. Andrews, M. Mansuripur, C. Denz, C. Alpmann, P. Banzer, T. Bauer, E. Karimi, L. Marrucci, M. Padgett, M. Ritsch-Marte, N. M. Litchinitser, N. P. Bigelow, C. Rosales-Guzmán, A. Belmonte, J. P. Torres, T. W. Neely, M. Baker, R. Gordon, A. B. Stilgoe, J. Romero, A. G. White, R. Fickler, A. E. Willner, G. Xie, B. McMorran, and A. M. Weiner, J. Opt. **19**, 013001 (2017).

[2] K. Volke-Sepulveda, V. Garcés-Chávez, S. Chávez-Cerda, J. Arlt, and K. Dholakia, J. Opt. B **4**, S82 (2002).

[3] V. Garcés-Chávez, D. McGloin, M. J. Padgett, W. Dultz, H. Schmitzer, and K. Dholakia, Phys. Rev. Lett. **91**, 093602 (2003).

[4] D. McGloin, V. Garcés-Chávez, and K. Dholakia, Opt. Lett. **28**, 657 (2003).

[5] R. Jáuregui and S. Hacyan, Phys. Rev. A **71**, 033411 (2005).

[6] G. Thirunavukkarasu, M. Mousley, M. Babiker, and J. Yuan, Philos. Trans. R. Soc. A **375**, 20150438 (2017).

[7] A. F. Rañada, Lett. Math. Phys. **18**, 97 (1989).

[8] A. F. Rañada and J. Trueba, Phys. Lett. A **202**, 337 (1995).

[9] A. Ranada and J. Trueba, Nature (London) **384**, 124 (1996).

[10] R. P. Cameron, S. M. Barnett, and A. M. Yao, New J. Phys. **14**, 053050 (2012).

[11] I. Fernandez-Corbaton, X. Zambrana-Puyalto, and G. Molina-Terriza, Phys. Rev. A **86**, 042103 (2012).

[12] G. Afanasiev and Y. P. Stepanovsky, Nuovo Cimento A **109**, 271 (1996).

[13] K. Y. Bliokh and F. Nori, Phys. Rev. A **83**, 021803(R) (2011).

[14] M. M. Coles and D. L. Andrews, Phys. Rev. A **85**, 063810 (2012).

[15] F. Crimin, N. Mackinnon, J. Götte, and S. Barnett, Appl. Sci. **9**, 828 (2019).

[16] F. Crimin, N. Mackinnon, J. Götte, and S. Barnett, J. Opt. **21**, 094003 (2019).

[17] S. Nechayev, J. S. Eismann, R. Alaee, E. Karimi, R. W. Boyd, and P. Banzer, Phys. Rev. A **103**, L031501 (2021).

[18] K. A. Forbes and G. A. Jones, J. Opt. **23**, 115401 (2021).

[19] K. Koksal, M. Babiker, V. E. Lembessis, and J. Yuan, J. Opt. Soc. Am. B **39**, 459 (2022).

[20] P. Woźniak, I. De Leon, K. Höflich, G. Leuchs, and P. Banzer, Optica **6**, 961 (2019).

[21] L. Allen, M. Padgett, and M. Babiker, Prog. Opt. **39**, 291 (1999).

[22] A. Aiello, N. Lindlein, C. Marquardt, and G. Leuchs, Phys. Rev. Lett. **103**, 100401 (2009).

[23] X. Piao, S. Yu, and N. Park, Phys. Rev. Lett. **120**, 203901 (2018).